CHAPTER 4

Optimal Trajectory Tracking in Approaching

During the mission of a TSR, the operation robot should arrive at the appointed position and maintain stable relative attitude before on-orbit service. Therefore an optimal mode (minimum fuel or flight time) is necessary for this process. However, the fuel of the operation robot is limited. To save thruster fuel, this chapter proposes a coordinated orbit control and attitude stability method for tracking the optimal approach trajectory based on the space tether and actuators of the operation robot.

The optimal trajectory planning problem is an optimal control process that is under some restricted conditions, such as path, control, or other constraints. Fuel consumption or approach time is usually chosen as the optimal index. Ulybyshev presented a trajectory optimization method for low-thrust spacecraft that used the discretization of a spacecraft trajectory on segments and sets of pseudoimpulses for each segment [1,2]. Suzuki presented a sequential goal programming approach that considered not only well-defined flight trajectory problems but also ill-defined problems [3]. An interval optimization was proposed according to the fixed-time multiple impulse rendezvous problem [4]. The methods mentioned here represent the development of optimal control problems in recent years. However, they focused on long-distance optimal trajectory planning.

The pseudospectral method [5–7] is a popular direct method that parameterizes the state and control variables using orthogonal polynomials such as the Legendre and Chebyschev polynomial. It approximates the dynamics at various quadrature points, such as the Legendre-Gauss (LG), Legendre-Gauss-Radau (LGR), and Legendre-Gauss-Lobatto (LGL) points [8]. The use of global polynomials, together with the Gauss quadrature collocation points, is known to provide accurate approximations that converge exponentially [8]. Therefore this method is widely used for many trajectory optimization applications.

For coordinated control, Nakamura et al. discussed the collaborative control of the tension and thruster in approaching the target of a tethered

https://doi.org/10.1016/B978-0-12-812309-6.00004-X

retriever, but the attitude is not considered [9]. Nohmi designed a space robot that is connected to a mother spacecraft through a tether. The tethered subsystem's attitude can be controlled by the tether tension through its link motion [10]. The necessary initial momentum for the space robot is generated by the spacecraft-mounted manipulator, and its trajectory is adjusted by controlling tether tension [11]. Mori proposed the concept of tethered satellite cluster systems and established the coordinated control method using tension and thrust, which decreased thruster fuel [12]. A coordinated fault-tolerant nonlinear control design was presented by Godard et al. [13] to control the attitude of a satellite using movement of the tether attachment points. A TSR is similar in concept to this research. However, these researchers only considered either orbit control or attitude control through tension force of tether. When attitude and orbit control through tether are considered at the same time, it becomes a more complex coupled problem.

In this chapter, the optimal trajectory for approaching a target is designed based on Gauss pseudospectral method. To save the thrust fuel of the operation robot, this chapter presents a coordinated orbit control and attitude stability method for tracking the optimal approach trajectory. The Gauss pseudospectral method is a suitable trajectory planning method for continuous control force because of its global convergent characteristics. In a coordinated control method, the space tether and thrusters are used to control the position of operation robot; the reaction wheels keep the attitude stable. The idea of optimization and distribution of control force is provided for the first time. By applying distributive tension force, the thruster fuel is saved. The disturbed torque of the space tether is unknown, which can be estimated and compensated by reaction wheels through a time-delay algorithm. Therefore the complex coupled control problem can be converted to a simple decoupled control by utilizing this coordinated control, and it can save thruster fuel at the same time.

The traditional control method for tracking optimal trajectory is PID (or PD) feedback control associated with feedforward control based on an optimal trajectory planning model. The control force can be realized by thrusters, and the attitude can be stabilized by a thruster or reaction wheel through a common PD (or PID) control method. Compared with this traditional method, the coordinated control method of this chapter proposed the idea of distributing the optimal control force to the thrusters and space tether through the approaching process, and the attitude angles can be stabilized by reaction wheels through a time-delay algorithm. Therefore the highlights of the coordinated control method are taking full use of the space

tether and overcoming an uncertain influence on attitude angles by the space tether. Saving thruster fuel is an advantage in practical applications.

4.1 TRAJECTORY MODELING IN APPROACHING

The target satellite is assumed to fly in a circular orbit, and the influence of the perturbation is not taken into account. The well-known Clohessy-Wiltshire equation is used to describe the motion of the operation robot. The reference frames are shown in Fig. 4.1, which include the target orbit frame $oxyz$. The target orbit plane is oxz. The C-W equation is illustrated by Eq. (4.1), where a_x, a_y, and a_z denote the thrust acceleration of the operation robot, x, y, and z are the positions of the operation robot in $oxyz$ frame, $\dot{x}$, $\dot{y}$, and $\dot{z}$ are relative velocities of the operation robot in $oxyz$ frame, ω_t is the orbital angular rate of the target. State variables are expressed by $X = [x, y, z, \dot{x}, \dot{y}, \dot{z}]^{\mathrm{T}}$, and the control force can be written by $\boldsymbol{u} = \left[ma_x, ma_y, ma_z\right]^{\mathrm{T}}$, where m is the mass of operation robot.

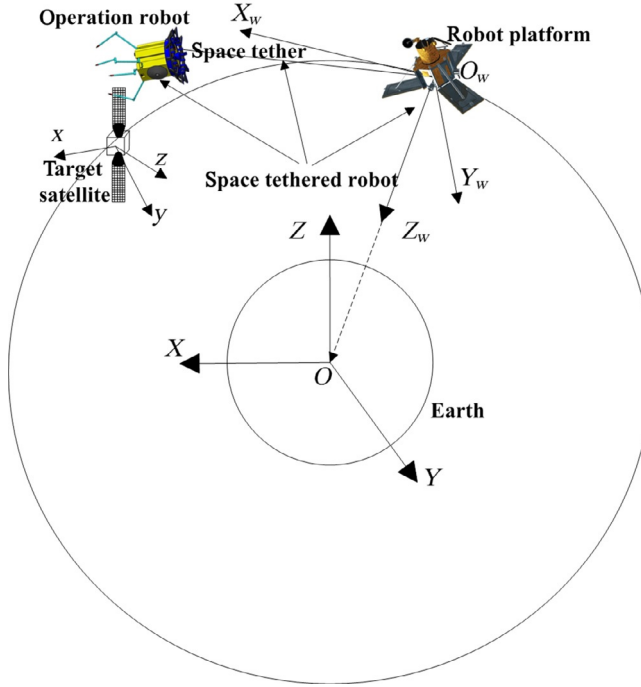

Fig. 4.1 The required reference frame of a space-tethered robot system.

$$\begin{cases} \ddot{x} - 2\omega_t \dot{z} = a_x \\ \ddot{y} + {\omega_t}^2 y = a_y \\ \ddot{z} + 2\omega_t \dot{x} - 3{\omega_t}^2 z = a_z \end{cases} \tag{4.1}$$

According to the statements above, the dynamics equation of the operation robot in Eq. (4.1) can be rewritten in a more compact form:

$$\dot{\boldsymbol{X}} = \boldsymbol{f}(\boldsymbol{X}, \boldsymbol{u}, t)\dot{\boldsymbol{X}} = \boldsymbol{f}(\boldsymbol{X}, \boldsymbol{u}, t) \tag{4.2}$$

where $\boldsymbol{f}$ in Eq. (4.1) is the function of derivatives of the state variables, control variables, state variables, and time. Control constraints must be enforced because the thrusters produce control force that is bounded by $F_{\max}$.

$$\begin{cases} -F_{\max} \le u_x \le F_{\max} \\ -F_{\max} \le u_y \le F_{\max} \\ -F_{\max} \le u_z \le F_{\max} \end{cases} \tag{4.3}$$

where $u_x = ma_x$, $u_y = ma_y$, and $u_z = ma_z$. The minus "−" denotes the direction of the control force.

The optimal solution should satisfy the appointed terminal constraints, which are represented by Eq. (4.4). In this chapter, the operation robot should arrive the terminal point, which must match the position and velocity relative at the arrival time t_f, which can be expressed by the form:

$$\boldsymbol{\Phi}\big(\boldsymbol{X}\big(t_f\big)\big) = 0 \tag{4.4}$$

where $\boldsymbol{\Phi}$ is the function of the terminal constraint. Before the operation robot is released by the robot platform, the space-tethered robot system will have already arrived at the same orbit with target, and the relative distance between the robot platform and the target are at the 200 m level. Furthermore, the thruster fuel of operation robot is limited. Therefore, minimal fuel consumption is preferential; the approach time t_f is not optimized. The trajectory optimization performance index J_1 is written as:

$$J_1 = \int_{t_0}^{t_f} \boldsymbol{u}^{\mathrm{T}}(t)\boldsymbol{u}(t)dt \tag{4.5}$$

The initial conditions of the operation robot are $\boldsymbol{X}(t_0) = \boldsymbol{X}_0$, and to make the optimal trajectory design problem well defined; the path constraints are expressed as follows:

$$\boldsymbol{X}_{\min} \le \boldsymbol{X} \le \boldsymbol{X}_{\max} \tag{4.6}$$

where $\boldsymbol{X}_{\min}$ and $\boldsymbol{X}_{\max}$ are the minimum and maximum of state variables separately.

Thus the basic task is now to design an optimal trajectory satisfying the differential constraints in Eq. (4.2), the control constraints in Eq. (4.3), the initial conditions $\boldsymbol{X}_0$, the terminal constrains in Eq. (4.4) and the path constrains in Eq. (4.6), and at the same time minimizing the performance index in Eq. (4.5) as small as possible.

The optimal approaching trajectory of the operation robot is designed via the pseudospectral method. The pseudospectral method in the trajectory optimization is a special scheme that transcribes a continuous dynamic optimization problem to a nonlinear programming (NLP) problem, which are among the various orthogonal polynomials utilized by the pseudospectral method that are all defined in the normalized domain $[-1,1]$. First, the time domain is transformed by introducing the following equation:

$$\tau = \frac{2t}{t_f - t_0} - \frac{t_f + t_0}{t_f - t_0} \tag{4.7}$$

where $\tau \in [-1,1]$ is the normalized time. Thus the dynamics of operation robot in Eq. (4.2) can be converted into:

$$\frac{d}{d\tau}\boldsymbol{X} = \frac{t_f - t_0}{2}\boldsymbol{f}(\boldsymbol{X}, \boldsymbol{u}, \tau) \tag{4.8}$$

The state variables $\boldsymbol{X}$ can be approximated by Lagrange interpolation, which can be written as:

$$\boldsymbol{X}(\tau) = \sum_{i=0}^{M} L_i(\tau)\boldsymbol{X}(\tau_i) \tag{4.9}$$

where $L_i(\tau) = \prod_{j=0, j\neq i}^{M} \frac{\tau - \tau_j}{\tau_i - \tau_j}$ is the Lagrange interpolation polynomial based on the Legendre-Gauss (LG) point τ_h, $h = 1, 2, \ldots, M$, and point $\tau_0 = -1$ is appended by the Gauss pseudospectral method. And the LG point τ_h are the roots of:

$$P_M(\tau) = \frac{1}{2^M M!}\frac{d^M}{d\tau^M}\left[\left(\tau^2 - 1\right)^M\right] = 0 \tag{4.10}$$

However, the state variables $\boldsymbol{X}(\tau)$ do not contain the discrete point at operation time $\tau_f = 1$. Thus the final variable can be discretized and approximated via the Gauss quadrature.

$$\boldsymbol{X}(\tau_f) - \boldsymbol{X}(\tau_0) - \frac{t_f - t_0}{2}\sum_{i=1}^{M} \omega_i \boldsymbol{f}\left(\boldsymbol{X}(\tau_i), \boldsymbol{U}(\tau_i), \tau_i;\, t_0, t_f\right) = 0 \tag{4.11}$$

where $\omega_i = \dfrac{2}{(1-\tau_i^2)\left[\dot{P}_M(\tau_i)\right]^2}$, $i = 1, 2, \ldots, M$ denote the Gauss weights and $\boldsymbol{U}(\tau_i)$ the approximation of discrete control force. The control variables $\boldsymbol{u}$ are then approximated by Lagrange interpolation:

$$\boldsymbol{u}(\tau) = \sum_{i=1}^{M} \widetilde{L}_i(\tau)\boldsymbol{U}(\tau_i) \tag{4.12}$$

where $\widetilde{L}_i(\tau) = \prod_{j=1, j\neq i}^{M} \dfrac{\tau - \tau_j}{\tau_i - \tau_j}$ is the Lagrange interpolation polynomial based on the Legendre-Gauss (LG) point τ_h, $h = 1, 2, \ldots, M$. The derivatives of the state variables $\boldsymbol{X}(\tau)$ are estimated by differentiating Eq. (4.9).

$$\frac{d\boldsymbol{X}(\tau_k)}{d\tau} = \sum_{i=0}^{M} \dot{L}_i(\tau_k)\boldsymbol{X}(\tau_i) = \sum_{i=0}^{M} D_{ki}\boldsymbol{X}(\tau_i), \quad (k = 1, 2, \ldots, M) \tag{4.13}$$

where $D_{ki} = \dot{L}_i(\tau_k) = \sum_{l=0}^{M} \left(\prod_{j=0, j\neq i, l}^{M} (\tau_k - \tau_j) \Big/ \prod_{j=0, j\neq i}^{M} (\tau_i - \tau_j) \right)$, which are the elements of the $M \times (M+1)$ differentiation matrix $\boldsymbol{D}$.

The relative dynamics of the operation robot can be approximated by imposing it at some specific nodes. At these nodes, the following equations are satisfied:

$$\boldsymbol{R}_k = \sum_{i=0}^{M} D_{ki}\boldsymbol{X}_i - \frac{t_f - t_0}{2} f\left(\boldsymbol{X}_k, \boldsymbol{U}_k, \tau_k; t_0, t_f\right) = 0, \quad (k = 1, \ldots, M) \tag{4.14}$$

Thus the algebraic constrains are imposed by the LG point τ_k, $k = 1, 2, \ldots, M$. And the boundary constraints, path constraints, and control constraints are written directly as:

$$\boldsymbol{X}(-1) = \boldsymbol{X}_0, \quad \boldsymbol{\Phi}(\boldsymbol{X}(1)) = 0 \tag{4.15}$$

$$\boldsymbol{X}_{\min} \leq \boldsymbol{X}(\tau_k) \leq \boldsymbol{X}_{\max} \tag{4.16}$$

$$\begin{cases} -F_{\max} \leq \boldsymbol{u}(\tau_k)_x \leq F_{\max} \\ -F_{\max} \leq \boldsymbol{u}(\tau_k)_y \leq F_{\max} \\ -F_{\max} \leq \boldsymbol{u}(\tau_k)_z \leq F_{\max} \end{cases} \tag{4.17}$$

where $\boldsymbol{u}(\tau_k)_x$, $\boldsymbol{u}(\tau_k)_y$, and $\boldsymbol{u}(\tau_k)_z$ are the control force of the x-axis, y-axis, and z-axis of $oxyz$ frame.

The energy optimal performance index J_1 is discretized as:

$$J_1 = \frac{t_f - t_0}{2} \int_{-1}^{1} \boldsymbol{u}^{\mathrm{T}}(\tau)\boldsymbol{u}(\tau)d\tau = \frac{t_f - t_0}{2} \sum_{k=1}^{M} \boldsymbol{U}^{\mathrm{T}}(\tau_k)\boldsymbol{U}(\tau_k)\omega_k \tag{4.18}$$

Therefore the object function in Eq. (4.18) and the various constraints in Eqs. (4.11), (4.14)–(4.17) finally formulate the original continuous optimization problem as an NLP. The optimized state variables $\boldsymbol{X}(\tau_i)$, $i=0,1,2,\ldots,M$ and the control force $\boldsymbol{U}(\tau_k)$, $k=1,2,\ldots,M$. These parameters can be solved by SNOPT optimization algorithm and corresponding software [14]. And the optimal discrete control force $\boldsymbol{U}(\tau_k)$ and optimal discrete trajectory $\boldsymbol{X}(\tau_i)$ are obtained. The continuous optimal control force and trajectory are obtained via Lagrange interpolation towards discrete points.

4.2 COORDINATED CONTROL METHOD

In order to save the thrust fuel consumption, this section investigates the coordinated orbit and attitude control method using thrusters, reaction wheels, and a space tether. The reaction wheels consume electricity, obtained from the robot platform through the space tether, thus, electricity consumption is ignored. The environmental interference, sensor measurement error, and actuator exerting error are also ignored.

The coordinated control diagram is shown in Fig. 4.2.

The overall process is:

Step 1: The optimal continuous orbit control force is obtained from the discrete control force using the Gauss pseudospectral method via interpolation scheme.

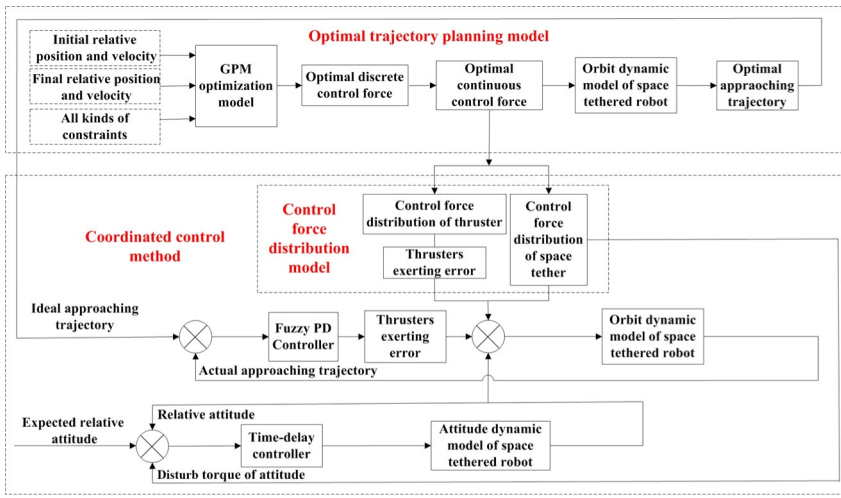

Fig. 4.2 Coordinated control diagram of TSR.

Step 2: The characteristics of the tension force is analyzed, and the distributive control force of the tether and the three direction thrusts are obtained by minimizing thruster fuel (the robot platform supplies tether's tension force). The optimal distribution control force of the thrusters and space tether are given to coordinated control model. By comparing between the ideal trajectory and actual relative position of the operation robot, the fuzzy PD controller is designed in order to tracking the optimal approaching trajectory.

Step 3: The relative attitude interferential torque is obtained by analyzing the connection point between the space tether and the operation robot, and the relative attitude is stabilized using the coordinated time-delay algorithm through the reaction wheels.

4.2.1 Optimization and Distribution of the Orbit Control Force

The aim of this section is to optimize and distribute the control force to the space tether and thrusters. The entire space-tethered robot system is complex for the existence of the tether. Therefore the following assumptions are made:

(1) The space tether is massless and inextensible.
(2) The tension force is supplied by releasing or retrieving the tether for the rolling motor.
(3) The tether is capable of exerting force along straight line connecting the robot platform and the operation robot.
(4) The robot platform moves in the same orbit with the target satellite before releasing the operation robot through space tether.
(5) The tether's influence on the robot platform is ignored.

The coordinated control scheme of the operation robot is shown in Fig. 4.3. O_txyz is the target orbit frame, $\boldsymbol{O_tO_m}$ is the projection vector in O_txz plane of the position vector for the operation robot in the O_txyz frame, $\boldsymbol{O_tO_w}$ is projection vector in the O_txz plane of the position vector for the robot platform in O_txyz frame, $\boldsymbol{O_mO_w}$ is the projection vector in the O_txz plane of the vector where the operation robot pointed to the robot platform in the O_txyz (angle α is between $\boldsymbol{O_mO_w}$ and the tether's direction), β is the angle between $\boldsymbol{O_mO_w}$ and $\boldsymbol{O_tO}$. Therefore it has:

$$\boldsymbol{O_mO_w} = \boldsymbol{O_tO_w} - \boldsymbol{O_tO_m} \tag{4.19}$$

F_x, F_y, and F_z are the optimal continuous control force obtained by the Gauss pseudospectral method via the interpolation scheme. F_t is assumed to be the tension force of the space tether after distributing control force.

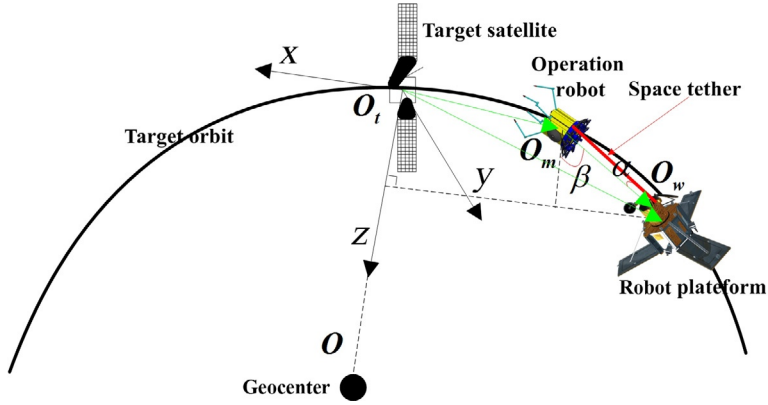

Fig. 4.3 Coordinated control of the operation robot.

Meanwhile, F_{xs}, F_{ys}, and F_{zs} are the distribution control forces of the thrusters in $x/y/z$ three directions. Therefore we have:

$$F_{xs} = F_x - F_t \cos\alpha \sin\beta \tag{4.20}$$

$$F_{ys} = F_y - F_t \sin\alpha \tag{4.21}$$

$$F_{zs} = F_z - F_t \cos\alpha \cos\beta \tag{4.22}$$

The unit vector along the tether direction is obtained according to the geometric relationship:

$$[i_x \quad i_y \quad i_z]^{\mathrm{T}} = \frac{\boldsymbol{O_m O_w}}{|\boldsymbol{O_m O_w}|} \tag{4.23}$$

$$\tan\beta = \frac{i_x}{i_z} \tag{4.24}$$

According to the actual situation of the operation robot during the approaching target phase, the motion of the out-of-plane (y direction) is ignored. Therefore the cost function of the optimization and distribution control force is chosen as follows:

$$J_f = w_1 F_{xs} + w_2 F_{zs} \tag{4.25}$$

where w_1 and w_2 are the weight coefficients, which can minimize the cost function and distribute the control force to the space tether and thrusters at the same time. The weight coefficients w_1 and w_2 are decided by the direction of releasing operation robot. If the operation robot is released in the

x-axis direction, $0 < w_2 < w_1 < 1$. If the operation robot is released in the z-axis direction, $0 < w_1 < w_2 < 1$.

In this section, the simulated annealing algorithm is used to optimize and distribute the control force. The simulated annealing algorithm was adopted to control force optimization and distribution. The control force was optimized and distributed in discrete time point, and the continuous distribution of the control force was obtained through polynomial fitting because of the low optimization speed of simulated annealing algorithm.

The simulated annealing algorithm was derived from the solid annealing principle based on the Monte Carlo iterative method for heuristic searching, which was theoretically proven to converge for global optimization in theory. Its control parameters include initial temperature T_0, minimum temperature $T_{\min}$, iteration number n, annealing coefficient ξ, and stopping condition. The detail of process can be seen in Ref. [15].

The interferential torque is related to the tension force and the connection point between the tether and the operation robot. It is assumed that the distance between the connection point and the centroid of the operation robot is l_x, l_y, and l_z in the body frame. The interferential torque $\boldsymbol{T}_t$ can be estimated by Eq. (4.26)

$$\boldsymbol{T}_t = \boldsymbol{l}^{\times}\boldsymbol{F}_t, \quad \boldsymbol{l}^{\times} = \begin{bmatrix} 0 & -l_z & l_y \\ l_z & 0 & -l_x \\ -l_y & l_x & 0 \end{bmatrix} \tag{4.26}$$

4.2.2 Tether Reeling Model and Tether's Tension Force Controller

A space tether can be used to supply the tension force that is distributed by the proposed method. The Tether control mechanism is usually mounted on the Robot platform, which consists of a reel, reel drive motor, and a reel lock unit. The operation robot is released through this mechanism. The tether's undeformed length l is regulated by the angular velocity ω of the reel. Thus the actual length l_a of a space tether can be calculated by the geometrical relationship between the robot platform and the operation robot. Therefore the tension F_l of the tether is given as:

$$F_l = \begin{cases} \dfrac{EA(l-l_a)}{l} + \dfrac{EAC(\dot{l}-\dot{l}_a)}{l} & l < l_a \\ 0 & l > l_a \end{cases} \tag{4.27}$$

where E, A, and C represent Young's modulus, a cross-sectional area, and viscous damping coefficient of the tether, respectively.

Assume r to be the radius of the reel, therefore, the relationship between l and ω can be obtained:

$$l = \int_{t_0}^{t_f} \omega \cdot r dt \tag{4.28}$$

The F_l have been obtained through a control force optimization algorithm. Therefore the rotated angular velocity ω can be calculated by Eqs. (4.27) and (4.28).

4.2.3 Fuzzy PD Controller for Tracking Optimal Trajectory

Generally, the Fuzzy logic control is adapted to the uncertain control problem [16]. Therefore the Fuzzy PD control is selected because of the thrusters' uncertain errors in this chapter. The Fuzzy PD controller is designed by Eq. (4.30), where, $\boldsymbol{e}$ is the position error, $\boldsymbol{k}_p$ and $\boldsymbol{k}_d$ are the corresponding coefficients separately. $\boldsymbol{u}$ is the control vector of the x-, y-, and z-axis directions in the target orbit coordinate frame.

$$\boldsymbol{u}(k) = \boldsymbol{k}_p \boldsymbol{e}(k) + \boldsymbol{k}_d [\boldsymbol{e}(k) - \boldsymbol{e}(k-1)] \tag{4.29}$$

In Eq. (4.29), $\boldsymbol{k}_p = \boldsymbol{k}_{p_0} + \boldsymbol{k}'_p$, $\boldsymbol{k}_d = \boldsymbol{k}_{d_0} + \boldsymbol{k}'_d$, $\boldsymbol{k}_{p_0}$, and $\boldsymbol{k}_{d_0}$ are static coefficient, which are defined previously. $\boldsymbol{k}'_p$ and $\boldsymbol{k}'_d$ are tuned on line by Fuzzy rules.

In the coordinated control method, the optimal distributing control force of the thrusters and space tether are given to the control model. Therefore the operation robot can track the optimal approaching trajectory accurately with the help of Fuzzy PD controller.

4.3 ATTITUDE STABILITY STRATEGY

4.3.1 Design of the Attitude Controller

$\boldsymbol{\omega}_c = [\omega_{cx} \ \ \omega_{cy} \ \ \omega_{cz}]^{\mathrm{T}}$ is defined as the operation robot angular velocity vector. The operation robot relative attitude kinematics equation is established using relative attitude quaternion in this chapter. This chapter also defines $\boldsymbol{q}_r = [q_1 \ \ q_2 \ \ q_3]^{\mathrm{T}}$ and $\boldsymbol{Q}_r = \left[q_0 \ \ \boldsymbol{q}_r{}^{\mathrm{T}}\right]^{\mathrm{T}}$, which satisfy $q_0^2 + q_1^2 + q_2^2 + q_3^2 = 1$. $\boldsymbol{Q}_r$ is relative attitude quaternion of operation robot. Thus the operation robot relative attitude quaternion kinematics equation is obtained by:

$$\dot{\boldsymbol{Q}}_r = \frac{1}{2} \boldsymbol{Q}_r{}^{\times} \boldsymbol{\omega}_r \tag{4.30}$$

where $\boldsymbol{\omega}_r$ is the operation robot rotation angular velocity relative to the target, $\boldsymbol{Q}_r^{\times} = \begin{bmatrix} -q_1 & -q_2 & -q_3 \\ q_0 & -q_3 & q_2 \\ q_3 & q_0 & -q_1 \\ -q_2 & q_1 & q_0 \end{bmatrix}$. The operation robot is provided with four reaction wheels, where three are installed by three inertia axes and the fourth is installed the position at the same angle as that of the other three.

Assume: $\boldsymbol{I}^c = \mathrm{diag}\left(I_x^c, I_y^c, I_z^c\right)$ is the inertia matrix of operation robot, $\boldsymbol{J}^w = \mathrm{diag}\left(J_1^w, J_2^w, J_3^w, J_4^w\right)$ is the inertia matrix of reaction wheels, $\boldsymbol{\Omega} = \begin{bmatrix} \Omega_1 & \Omega_2 & \Omega_3 & \Omega_4 \end{bmatrix}^{\mathrm{T}}$ is the angular velocity of reaction wheels relative to operation robot, $\boldsymbol{h}_w$ is the angular momentum vector of reaction wheels, $\boldsymbol{h}_b$ is the angular momentum vector of operation robot; $\boldsymbol{T}_d$ is the sum of solar radiation torque and pneumatic torque, $\boldsymbol{T}_t$ is the tether interferential torque to operation robot, $\boldsymbol{T}_w$ is the inertia axes torque which reaction wheels supply to the operation robot, $\boldsymbol{N}$ is the input transformed matrix representing influence on three inertia axes of each wheel, and $\boldsymbol{U} = \begin{bmatrix} u_1 & u_2 & u_3 & u_4 \end{bmatrix}^{\mathrm{T}}$ is the input torque vector of four reaction wheels. The operation robot attitude dynamic equation in the space-tethered robot system is obtained as:

$$\dot{\boldsymbol{h}}_b + \dot{\boldsymbol{h}}_w = \boldsymbol{T}_w + \boldsymbol{T}_t \tag{4.31}$$

where:

$$\boldsymbol{h}_b = \boldsymbol{I}^c \boldsymbol{\omega}_c \tag{4.32}$$

$$\boldsymbol{h}_w = \boldsymbol{N}\boldsymbol{J}^w\boldsymbol{N}^{\mathrm{T}}\boldsymbol{\omega}_c + \boldsymbol{N}\boldsymbol{J}^w\boldsymbol{\Omega} \tag{4.33}$$

$$\boldsymbol{T}_w = \boldsymbol{N}\boldsymbol{U} = \boldsymbol{N}\left(-\boldsymbol{J}^w\dot{\boldsymbol{\Omega}} - \boldsymbol{J}^w\boldsymbol{N}^{\mathrm{T}}\dot{\boldsymbol{\omega}}_c\right) \tag{4.34}$$

The environmental torque is ignored. Let $\boldsymbol{\omega}_c^{\times} = \begin{bmatrix} 0 & -\omega_{cz} & \omega_{cy} \\ \omega_{cz} & 0 & -\omega_{cx} \\ -\omega_{cy} & \omega_{cx} & 0 \end{bmatrix}$. Thus the attitude dynamics equation can also be written as:

$$\boldsymbol{I}^c\dot{\boldsymbol{\omega}}_c + \boldsymbol{\omega}_c^{\times}\left(\boldsymbol{I}^c\boldsymbol{\omega}_c + \boldsymbol{N}\boldsymbol{J}^w\boldsymbol{N}^{\mathrm{T}}\boldsymbol{\omega}_c + \boldsymbol{N}\boldsymbol{J}^w\boldsymbol{\Omega}\right) = T_t + T_w \tag{4.35}$$

The relative attitude interferential torque is produced when there exists tension force exerted on the operation robot. Thus attitude stability is an important aspect in the coordinated control method. This chapter intends to control and stabilize the relative attitude using a time-delay algorithm through the reaction wheels of the operation robot.

The time-delay control method mainly deals with uncertainties and disturbances without any explicit estimation [17–20]. The unknown

dynamics contain model changes are caused by external interference. In this method, the idea is to supply the first period control and compensate the control changes due to the tether torque interference.

The attitude dynamics equation of the operation robot is shown by Eq. (4.35), where the interferential torque $\boldsymbol{T}_t$ inevitably leads to a change in the attitude dynamic model. Thus it can utilize the control torque to compensate for the interference. This section presents the design of the time-delay controller. Eq. (4.36) can be rewritten equivalently:

$$\boldsymbol{I}^c\dot{\boldsymbol{\omega}}_c = \boldsymbol{N}\boldsymbol{U} + \boldsymbol{Y} \tag{4.36}$$

where $\boldsymbol{Y} = -\boldsymbol{\omega}_c^{\times}\left(\boldsymbol{I}^c\boldsymbol{\omega}_c + \boldsymbol{N}\boldsymbol{J}^w\boldsymbol{N}^{\mathrm{T}}\boldsymbol{\omega}_c + \boldsymbol{N}\boldsymbol{J}^w\boldsymbol{\Omega}\right) + \boldsymbol{T}_t$, which is uncertainty and estimated by the one-step previous control. The estimation is defined as $\hat{Y}$. Therefore Eq. (4.37) can be rewritten as:

$$\boldsymbol{Y} \approx \circ\boldsymbol{Y} = \boldsymbol{Y}(t-T) = \boldsymbol{I}^c\dot{\boldsymbol{\omega}}_c(t-T) - \boldsymbol{N}\boldsymbol{U}(t-T) \tag{4.37}$$

where T is the control period. To cancel out $\boldsymbol{Y}$, Eq. (4.37) can also be rewritten as:

$$\boldsymbol{U} = \boldsymbol{N}^{-}\left[\boldsymbol{I}^c\dot{\boldsymbol{\omega}}_c - \boldsymbol{Y}\right] \tag{4.38}$$

Combining Eqs. (4.37) and (4.38) yields:

$$\boldsymbol{U} = \boldsymbol{U}(t-T) + \boldsymbol{N}^{-}\boldsymbol{I}^c\left[\dot{\boldsymbol{\omega}}_c(t) - \dot{\boldsymbol{\omega}}_c(t-T)\right] \tag{4.39}$$

where, $\boldsymbol{N}^{-} = \boldsymbol{N}^{\mathrm{T}}\left[\boldsymbol{N}\boldsymbol{N}^{\mathrm{T}}\right]^{-1}$ is an arbitrary generalized inverse matrix of $\boldsymbol{N}$. From the relative attitude relationship, it can conclude that:

$$\boldsymbol{\omega}_r = \boldsymbol{\omega}_c - \boldsymbol{H}\boldsymbol{\omega}_t \tag{4.40}$$

where $\boldsymbol{\omega}_t$ is the target angular velocity, $\boldsymbol{H}$ is the transformation matrix from the target orbit coordinate frame to the body coordinate frame of the operation robot.

$$\boldsymbol{H} = \begin{bmatrix} q_0^2 + q_1^2 - q_2^2 - q_3^2 & 2q_0q_3 + 2q_1q_2 & -2q_0q_2 + 2q_1q_3 \\ -2q_0q_3 + 2q_1q_2 & q_0^2 - q_1^2 + q_2^2 - q_3^2 & 2q_0q_1 + 2q_2q_3 \\ 2q_0q_2 + 2q_1q_3 & -2q_0q_1 + 2q_2q_3 & q_0^2 - q_1^2 - q_2^2 + q_3^2 \end{bmatrix} \tag{4.41}$$

In order to satisfy $\mathbf{Q}_r \to \mathbf{Q}_{rd}$ and $\boldsymbol{\omega}_r \to \boldsymbol{\omega}_{rd}$, the relative attitude and angular velocity are given by:

$$\begin{cases} \mathbf{Q}_{rd} = \mathbf{Q}_r + t_1\dot{\mathbf{Q}}_r \\ \boldsymbol{\omega}_{rd} = \boldsymbol{\omega}_r + t_2\dot{\boldsymbol{\omega}}_r \end{cases}, \quad (t_1 > t_2 > 0), \quad t_1 \text{ and } t_2 \text{ are time constants} \tag{4.42}$$

where t_1 and t_2 are time constants, those constants express the changing velocity. It is defined as $t_1 > t_2 > 0$, which means the angular velocity changes faster than the relative attitude.

The relationship between $\boldsymbol{\omega}_r$ and $\boldsymbol{Q}$ can be expressed by the attitude kinematic equation:

$$\dot{\boldsymbol{Q}}_r = \frac{1}{2}\boldsymbol{Q}_r^{\times}\boldsymbol{\omega}_r \Rightarrow \boldsymbol{\omega}_r = 2\left(\boldsymbol{Q}_r^{\times}\right)^{-}\dot{\boldsymbol{Q}}_r \tag{4.43}$$

where $\left(\boldsymbol{Q}_r^{\times}\right)^{-} = \left(\boldsymbol{Q}_r^{\times}\right)^{\mathrm{T}}\left[\left(\boldsymbol{Q}_r^{\times}\right)\left(\boldsymbol{Q}_r^{\times}\right)^{\mathrm{T}}\right]^{-1}$ is an arbitrary generalized inverse matrix of $\boldsymbol{Q}_r^{\times}$. It can obtain the relationship between $\dot{\boldsymbol{\omega}}_r$ and $\boldsymbol{Q}_r$ by combining Eqs. (4.42) and (4.43). Eq. (4.41) can be rewritten as:

$$\dot{\boldsymbol{\omega}}_r = \dot{\boldsymbol{\omega}}_c - \boldsymbol{H}\dot{\boldsymbol{\omega}}_t - \left(\frac{d\boldsymbol{H}}{dt}\right)\boldsymbol{\omega}_t \Rightarrow \dot{\boldsymbol{\omega}}_r = \dot{\boldsymbol{\omega}}_c + \boldsymbol{\omega}_r^{\times}\boldsymbol{\omega}_c \tag{4.44}$$

where $\boldsymbol{\omega}_r^{\times} = \begin{bmatrix} 0 & -\omega_{rz} & \omega_{ry} \\ \omega_{rz} & 0 & -\omega_{rx} \\ -\omega_{ry} & \omega_{rx} & 0 \end{bmatrix}$. By combining Eqs. (4.40), (4.43), and (4.444), the final time-delay attitude coordinated control law is:

$$\boldsymbol{U} = \boldsymbol{U}(t-T) + \boldsymbol{N}^{-}\boldsymbol{I}^{c}\left[\frac{2\left(\boldsymbol{Q}_r^{\times}\right)^{-}\frac{\boldsymbol{Q}_{rd}-\boldsymbol{Q}_r}{t_1} - \boldsymbol{\omega}_r}{t_2} - \boldsymbol{\omega}_r^{\times}\boldsymbol{\omega}_c - \dot{\boldsymbol{\omega}}_c(t-T)\right] \tag{4.45}$$

where $\boldsymbol{Q}_r$, $\boldsymbol{\omega}_r$, and $\boldsymbol{\omega}_c$ can be obtained by relative sensors, and the $\dot{\boldsymbol{\omega}}_c(t-T)$ can be estimated by:

$$\dot{\boldsymbol{\omega}}_c(t-T) = \frac{\boldsymbol{\omega}_c(t-T) - \boldsymbol{\omega}_c(t-2T)}{T} \tag{4.46}$$

However, the errors exist if we select Eq. (4.46). The $\dot{\boldsymbol{\omega}}_c(t-T)$ can be also expressed through Eqs. (4.42) and (4.44):

$$\dot{\boldsymbol{\omega}}_c(t-T) = \frac{2\left[\boldsymbol{Q}_r^{\times}(t-T)\right]^{-}\frac{\boldsymbol{Q}_{rd}-\boldsymbol{Q}_r(t-T)}{t_1} - \boldsymbol{\omega}_r(t-T)}{t_2} - \boldsymbol{\omega}_r(t-T)^{\times}\boldsymbol{\omega}_c(t-T) \tag{4.47}$$

4.3.2 Stability Proof of the Attitude Controller

The attitude control law in Eqs. (4.40) and (4.45) are stable under certain conditions.

Substituted Eq. (4.45) into (4.36) yields:

$$\begin{aligned}
&\boldsymbol{I}^c\dot{\boldsymbol{\omega}}_c+\boldsymbol{\omega}_c^{\times}\left(\boldsymbol{I}^c\boldsymbol{\omega}_c+\boldsymbol{N}\boldsymbol{J}^w\boldsymbol{N}^{\mathrm{T}}\boldsymbol{\omega}_c+\boldsymbol{N}\boldsymbol{J}^w\boldsymbol{\Omega}\right)\\
&\quad=\boldsymbol{T}_t+\boldsymbol{N}\boldsymbol{U}(t-T)+\boldsymbol{I}^c\left[\boldsymbol{\omega}_r(t-T)^{\times}\boldsymbol{\omega}_c(t-T)-\boldsymbol{\omega}_r{}^{\times}\boldsymbol{\omega}_c\right.\\
&\left.-\frac{2\left[\mathbf{Q}_r^{\times}(t-T)\right]^{-}\frac{\mathbf{Q}_{rd}-\mathbf{Q}_r(t-T)}{t_1}-\boldsymbol{\omega}_r(t-T)}{t_2}+\frac{2\left(\mathbf{Q}_r^{\times}\right)^{-}\frac{\mathbf{Q}_{rd}-\mathbf{Q}_r}{t_1}-\boldsymbol{\omega}_r}{t_2}\right]
\end{aligned}\tag{4.48}$$

The following equation is obtained from Eq. (4.36):

$$\begin{aligned}
\boldsymbol{N}\boldsymbol{U}(t-T)=&\boldsymbol{I}\dot{\boldsymbol{\omega}}_c(t-T)+\boldsymbol{\omega}_c^{\times}(t-T)\\
&\left[\boldsymbol{I}\boldsymbol{\omega}_c(t-T)+\boldsymbol{N}\boldsymbol{J}^w\boldsymbol{N}^{\mathrm{T}}\boldsymbol{\omega}_c(t-T)+\boldsymbol{N}\boldsymbol{J}^w\boldsymbol{\Omega}(t-T)\right]-\boldsymbol{T}_t
\end{aligned}\tag{4.49}$$

If we select a small value of the control period T, which satisfies:

$$\|\boldsymbol{\omega}_c-\boldsymbol{\omega}_c(t-T)\|_2\approx 0,\quad \|\boldsymbol{\Omega}-\boldsymbol{\Omega}(t-T)\|_2\approx 0 \tag{4.50}$$

The following equation can be obtained:

$$\boldsymbol{\omega}_c\approx\boldsymbol{\omega}_c(t-T),\quad \boldsymbol{\Omega}\approx\boldsymbol{\Omega}(t-T) \tag{4.51}$$

Substitute Eq. (4.49) into (4.48) and we have:

$$\begin{aligned}
&\boldsymbol{I}^c\dot{\boldsymbol{\omega}}_c-\boldsymbol{I}^c\dot{\boldsymbol{\omega}}_c(t-T)+\boldsymbol{\omega}_c^{\times}\left(\boldsymbol{I}^c\boldsymbol{\omega}_c+\boldsymbol{N}\boldsymbol{J}^w\boldsymbol{N}^{\mathrm{T}}\boldsymbol{\omega}_c+\boldsymbol{N}\boldsymbol{J}^w\boldsymbol{\Omega}\right)\\
&\quad=\boldsymbol{\omega}_c^{\times}(t-T)\left[\boldsymbol{I}^c\boldsymbol{\omega}_c(t-T)+\boldsymbol{N}\boldsymbol{J}^w\boldsymbol{N}^{\mathrm{T}}\boldsymbol{\omega}_c(t-T)+\boldsymbol{N}\boldsymbol{J}^w\boldsymbol{\Omega}(t-T)\right]\\
&\quad+\boldsymbol{I}^c\left[\frac{2\left(\mathbf{Q}_r^{\times}\right)^{-}\frac{\mathbf{Q}_{rd}-\mathbf{Q}_r}{t_1}-\boldsymbol{\omega}_r}{t_2}-\boldsymbol{\omega}_r^{\times}\boldsymbol{\omega}_c+\boldsymbol{\omega}_r(t-T)^{\times}\boldsymbol{\omega}_c(t-T)\right.\\
&\left.-\frac{2\left[\mathbf{Q}_r^{\times}(t-T)\right]^{-}\frac{\mathbf{Q}_{rd}-\mathbf{Q}_r(t-T)}{t_1}-\boldsymbol{\omega}_r(t-T)}{t_2}\right]
\end{aligned}\tag{4.52}$$

Substitute Eq. (4.51) into (4.2) and therefore, Eq. (4.52) can be simplified as:

$$\dot{\boldsymbol{\omega}}_c-\dot{\boldsymbol{\omega}}_c(t-T)\approx 0 \tag{4.53}$$

The $\boldsymbol{\omega}_c$ can be stable from Eq. (4.53), it can be expressed by $\dot{\boldsymbol{\omega}}_c=$ constant.

The following equation can be obtained by Eq. (4.42):

$$\boldsymbol{\omega}_r=\boldsymbol{\omega}_{rd}-t_2\dot{\boldsymbol{\omega}}_r \tag{4.54}$$

It is known that $\boldsymbol{\omega}_r$ is stable from Eq. (4.54), the static error is $t_2\dot{\boldsymbol{\omega}}_r$. Therefore the attitude control law is stable under Lyapunov stability conditions, and this completes the proof.

Now, we design the attitude PD control of the traditional control method in order to compare with the time-delay attitude control method. The attitude PD control law is shown in Eq. (4.54).

$$\boldsymbol{U} = \boldsymbol{N}^{-}\boldsymbol{I}^{c}\left[\boldsymbol{\omega}_{c}^{\times}\left(\boldsymbol{I}^{c}\boldsymbol{\omega}_{c} + \boldsymbol{N}\boldsymbol{J}^{w}\boldsymbol{N}^{\mathrm{T}}\boldsymbol{\omega}_{c} + \boldsymbol{N}\boldsymbol{J}^{w}\boldsymbol{\Omega}\right) - \boldsymbol{D}_1\boldsymbol{\omega}_{c} - \boldsymbol{D}_2\boldsymbol{M}(\boldsymbol{Q}_r - \boldsymbol{Q}_{rd})\right] \tag{4.55}$$

where $\boldsymbol{D}_1 = 2\xi\omega_n\boldsymbol{I}^{c}$ and $\boldsymbol{D}_2 = \omega_n^2\boldsymbol{I}^{c}$ are PD matrix parameters, ξ is the damping coefficient, ω_n is the frequency coefficient, $\boldsymbol{M} = \begin{bmatrix} 1 & 1 & 0 & 0 \\ 1 & 0 & 1 & 0 \\ 1 & 0 & 0 & 1 \end{bmatrix}$ is the equivalent transformed matrix of attitude quaternion.

Substitute Eq. (4.55) into (4.36):

$$\boldsymbol{I}^{c}\dot{\boldsymbol{\omega}}_{c} + 2\xi\omega_n\boldsymbol{I}^{c}\boldsymbol{\omega}_{c} + \omega_n^2\boldsymbol{I}^{c}\boldsymbol{M}(\boldsymbol{Q}_r - \boldsymbol{Q}_{rd}) = T_t \tag{4.56}$$

Eq. (4.55) expresses one kind of second-order system. However, if the disturbed attitude torque T_t existed, then the parameter ξ and ω_n should be selected in order to stabilize the attitude angles.

4.4 NUMERICAL SIMULATION

In the simulation, the traditional control method for tracking the optimal trajectory is compared with the proposed coordinated control method. The traditional control method consists of a PD controller associated with a feedforward control based on an optimal trajectory planning model, and the attitude can also be stabilized by a PD controller.

Assume: The operation robot is 10 kg and the robot platform is 2000 kg, $l_x = 0.3$ m, $l_y = 0.3$ m, $l_z = 0$ m, $\boldsymbol{X_0}$ is the best position relative to the target for releasing the operation robot, and $\boldsymbol{X_f} = (0 \;\; 0 \;\; 0 \;\; 0 \;\; 0 \;\; 0)^{\mathrm{T}}$ is the final desired position. $\boldsymbol{X_0} = (-244.35 \text{ m} \;\; 1 \text{ m/s} \;\; 0 \text{ m} \;\; 0 \text{ m/s} \;\; 0.0043 \text{ m} \;\; 0 \text{ m/s})^{\mathrm{T}}$. The maximum thruster force of each thruster is 0.3 N. $\boldsymbol{Q}_{r0}$ is the initial relative attitude of the operation robot and $\boldsymbol{Q}_d$ the desired relative attitude. $\boldsymbol{Q}_{r0} = [1 \;\; 0 \;\; 0 \;\; 0]^{\mathrm{T}}$ and $\boldsymbol{Q}_d = [1 \;\; 0 \;\; 0 \;\; 0]^{\mathrm{T}}$. It is assumed that the error of the control force generated by thruster is $\pm 0.02F$ (F is the desired control force). The mass of reaction wheel is 0.2 kg.

$$\boldsymbol{I}^c = \begin{bmatrix} 1.25 & -0.0025 & -0.00032 \\ -0.0025 & 1.15 & -0.00086 \\ -0.00032 & -0.00086 & 1.3 \end{bmatrix} \text{ kg m}^2,$$

$$\boldsymbol{J}^w = \begin{bmatrix} 0.005 & 0 & 0 & 0 \\ 0 & 0.005 & 0 & 0 \\ 0 & 0 & 0.005 & 0 \\ 0 & 0 & 0 & 0.005 \end{bmatrix} \text{ kg m}^2, \ \boldsymbol{N} = \begin{bmatrix} 1 & 0 & 0 & 1 \\ 0 & 1 & 0 & 1 \\ 0 & 0 & 1 & 1 \end{bmatrix}.$$

The rest of the parameters are shown in Table 4.1. The optimal trajectory for the operation robot during an approaching target phase is shown in Fig. 4.4. The optimal trajectory seems smooth, which means that the operation robot can track it easily. The operation robot can approach the target along the optimal trajectory accurately using the coordinated control method. Note that the offset in the z-axis direction are kept within ± 0.3 m, while nearly 0 m out of orbit plane. In the x-axis direction, the approaching trend is along the optimal trajectory. Therefore the operation robot can track the optimal trajectory effectively using the proposed coordinated control method.

Fig. 4.5 shows the space tether force obtained by optimization and distribution. FF is the optimal distributed tension force of a space tether in 0.1 s discrete time point using the simulated annealing algorithm. F is the optimal continuous tension force, obtained via cubic polynomial fitting for FF. The space tether can only supply tension force, as shown in Fig. 4.5. The trend of

Table 4.1 Relevant parameters of the operation robot

Optimization parameters	$T_0 = 100°C$, $T_{\min} = 0.01°C$, $n = 500$, $\xi = 0.85$, $w_1 = 0.8$, $w_2 = 0.2$	
Target orbit parameters	Orbit altitude $h = 622$ km, argument of perigee $w = 20$ degrees	True anomaly $f_t = 0.002$ degrees
Robot platform orbit parameters	Orbit inclination $i = 10$ degrees, eccentricity $e = 0$ Longitude ascending node $\Omega = 0$	True anomaly $f_c = 0$
Control parameters	$\boldsymbol{k}_{p_0} = \begin{bmatrix} 0.1 & 0 & 0 \\ 0 & 0.1 & 0 \\ 0 & 0 & 0.1 \end{bmatrix}$, $\boldsymbol{k}_{d_0} = \begin{bmatrix} 0.1 & 0 & 0 \\ 0 & 0.1 & 0 \\ 0 & 0 & 0.1 \end{bmatrix}$, $t_1 = 0.8$, $t_2 = 0.2$, $\xi = 0.7$, $\omega_n = 0.8$	
Tether and reel parameters	$EA = 25997$ N, $C = 0.3$, $r = 0.1$ m	

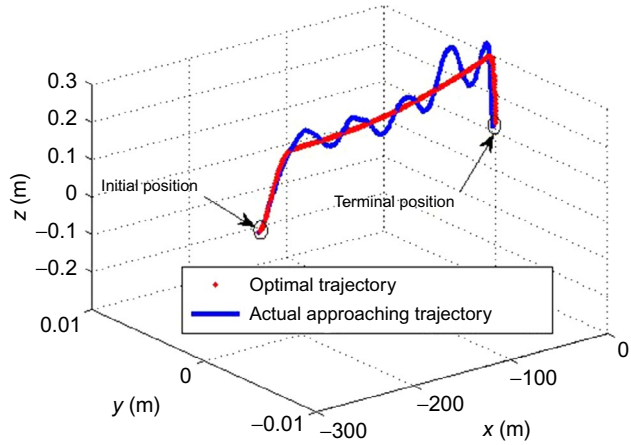

Fig. 4.4 Trajectory comparison for operation robot.

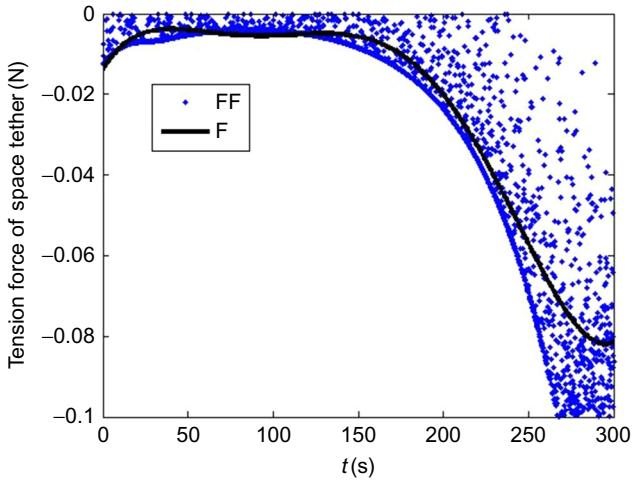

Fig. 4.5 Control force of a space tether.

the tension force is flat, thus, it can easily be imposed by the rolling reel and motor in the robot platform.

The thruster force comparison between the coordinated control and traditional control is shown in Figs. 4.6–4.8. The control force contains PD (or Fuzzy PD) control force and optimal control force is obtained from the trajectory planning model. Fig. 4.6 shows the control force comparison in the x-axis direction. The total approach time is 300 s. The coordinated thruster force contains distributive continuous force and Fuzzy PD control force.

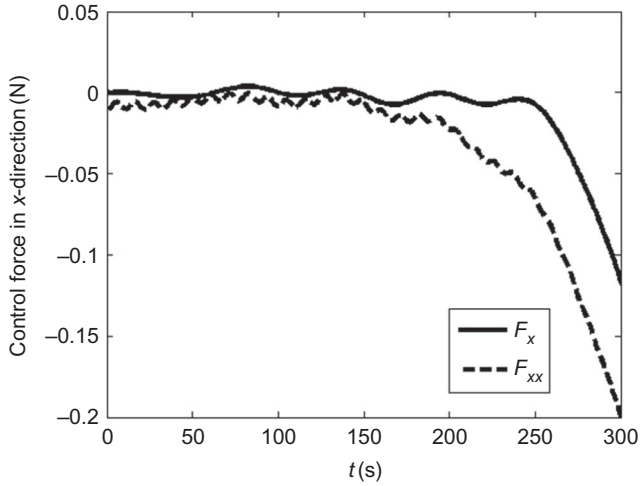

Fig. 4.6 Thruster force comparison in *x*-direction.

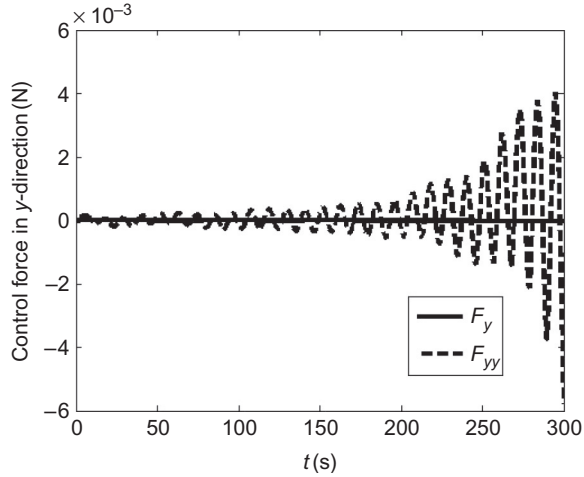

Fig. 4.7 Thruster force comparison in y-direction.

The distributive continuous force is obtained via a cubic polynomial fitting of an optimal distributive thruster force in 0.1 s discrete time point. F_x is the coordinated thruster force. The coordinated thruster force is less than 120 mN in the *x*-axis direction, otherwise, the traditional thruster force F_{xx} is less than 200 mN. Therefore this process can save thruster fuel significantly in the *x*-axis direction. Fig. 4.7 shows a control force comparison in the *y*-axis direction. The traditional control force (F_{yy}) is less than

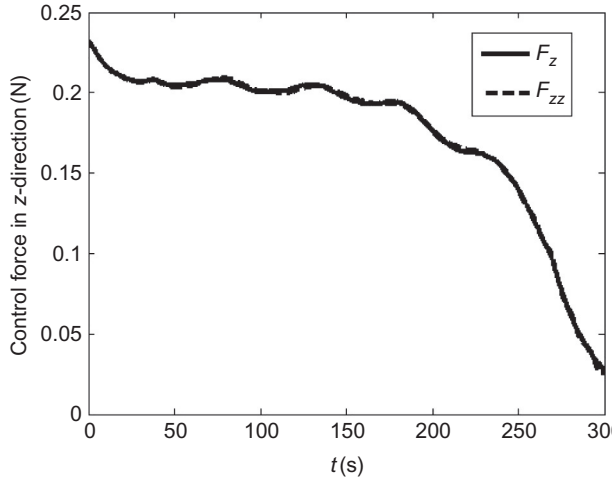

Fig. 4.8 Thruster force comparison in z-direction.

6×10^{-3} N, and the coordinated thruster force F_y is less than 5×10^{-4} N. The thruster fuel can be saved in the y-axis direction. Fig. 4.8 shows the control force comparison in the z-axis direction. F_z is the coordinated thruster force for tracking the optimal trajectory. F_{zz} is the traditional thruster force. In this simulation condition, F_{zz} is nearly equal to F_z, which express that it cannot save the thrust fuel in the z-axis direction. Because the operation robot is released in the z-axis direction, the control force of space tether are decided by the tether's direction.

Fig. 4.9 shows the thruster control force of Fuzzy PD controller of coordinated control. It takes thruster error into account. Except for the distributed control force or optimal force of thruster, the PD force of thruster is required to compensate error between the actual position and the optimal trajectory. The PD forces in all directions are kept between -10×10^{-3} and 6×10^{-3} N. The tether tension force can produce attitude interferential torque, because overlapping between the centroid of the operation robot and the connection point is difficult. Fig. 4.10 shows the interferential torque produced by the space tether. An interferential torque is presented in y- and z-axis directions. The attitude interferential torque is impossible to avoid because of the existing offset between the centroid of the operation robot and the connection point.

Fig. 4.11 shows the relative attitude angle using the coordinated attitude control method. The roll angle φ is about 0 degree. The yaw angle ψ and pitch angle θ are kept between -0.03 degrees and 0.03 degrees. Fig. 4.12

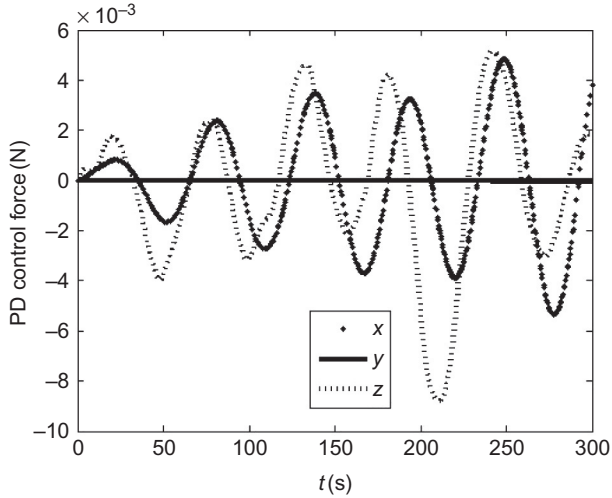

Fig. 4.9 Fuzzy PD control force of coordinated control.

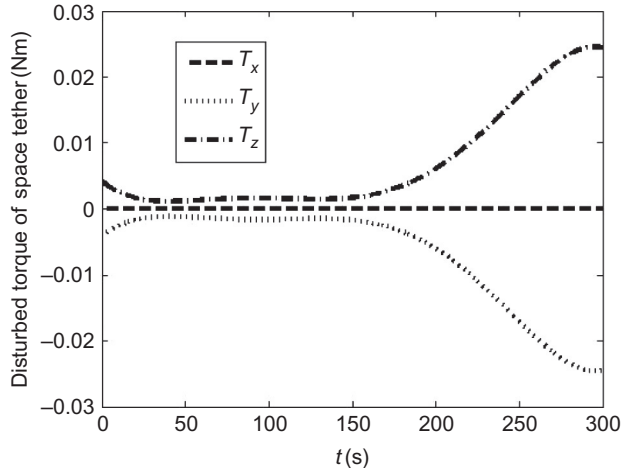

Fig. 4.10 Interferential torque produced by the space tether.

shows the relative attitude angle through the reaction wheels using the traditional attitude control method. The relative attitude angles are kept between −5 degrees and 5 degrees. Therefore the coordinated attitude control is better than the traditional attitude control at solving uncertain attitude control problems under tether interference.

The reaction wheels' angular velocity of coordinated control is shown in Fig. 4.13. In order to stabilize the relative attitude of operation robot, the

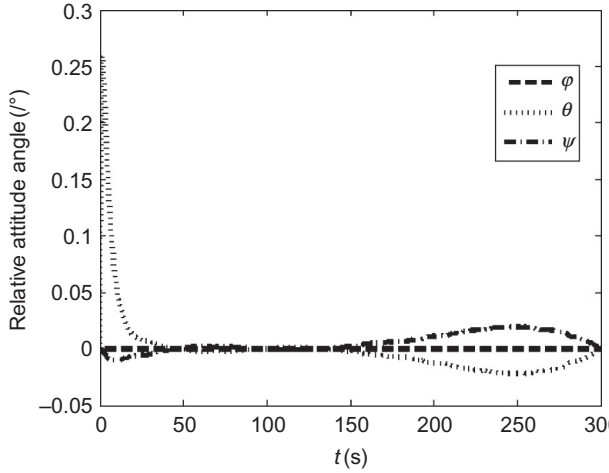

Fig. 4.11 Relative attitude angle of the operation robot for coordinated control.

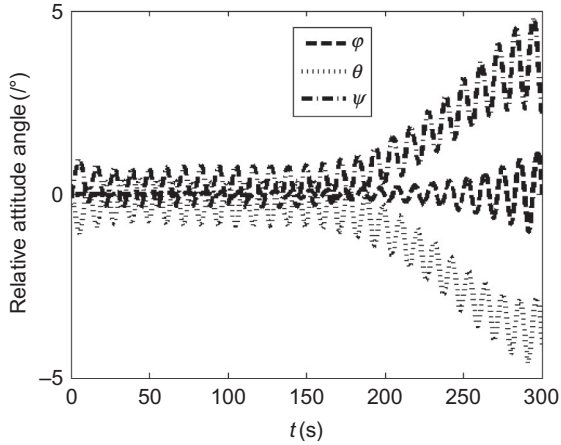

Fig. 4.12 Relative attitude angle of the operation robot for traditional control.

four reaction wheels work in the whole approach process. As is shown in Fig. 4.5, the distributive tension force of the space tether changes from 18 to 82 mN with the time, and the corresponding disturbed torque of the tether changes from 0.003 to 0.025 N m in Fig. 4.10. Therefore the compensated control torque of the time-delay controller cannot keep one constant value at last, and the angular velocity of the reaction wheels cannot maintain constant. However, the time-delay attitude controller is stable

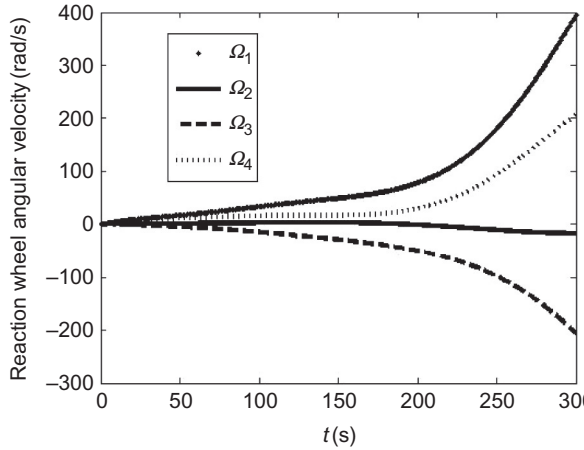

Fig. 4.13 Reaction wheels angular velocity of coordinated control.

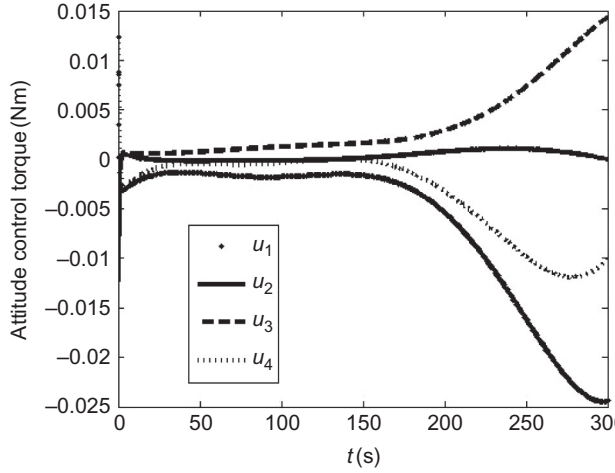

Fig. 4.14 Attitude control torque of coordinated control.

according to this special characteristic of the space-tethered robot system. The relative attitude and angular velocity of the operation robot can be kept stable, which can illustrate the stability of the attitude controller. Fig. 4.14 shows the attitude control torque of the coordinated control. The attitude control torques of the coordinated controls are kept between −0.025 and 0.015 N m.

REFERENCES

[1] Y. Ulybyshev, Trajectory optimization for spacecraft proximity operations with constraints, in: AIAA Guidance, Navigation, and Control Conference, Portland, Oregon, 2011.

[2] Y. Ulybyshev, Spacecraft trajectory optimization based on discrete sets of pseudo-impulses, in: AIAA/AAS Astrodynamics Specialist Conference and Exhibit, Honolulu, Hawaii, 2008.

[3] S. Suzuki, T. Yoshizawa, Multi-objective trajectory optimization by goal programming with fuzzy decisions, J. Guid. Control. Dyn. 17 (2) (1994) 297–303.

[4] E.V. Kampen, Q.P. Chu, J.A. Mulder, Optimization of spacecraft rendezvous and docking using interval analysis, in: AIAA Guidance, Navigation, and Control Conference, Toronto, Ontario Canada, 2010.

[5] D. Benson, A Gauss Pseudospectral Transcription for Optimal Control (Ph.D. thesis), Department of Aeronautics and Astronautics, Massachusetts Institute of Technology, USA, 2004.

[6] F. Fahroo, I.M. Ross, On discrete-time optimality conditions for pseudospectral methods, in: AIAA/AAS Astrodynamics Specialist Conference and Exhibit, Keystone, CO, 2006.

[7] T.D. Guo, F.H. Jiang, J.F. Li, Homotopic approach and pseudospectral method applied jointly to low thrust trajectory optimization, Acta Astronaut. 71 (2012) 38–50.

[8] D. Garg, M. Patterson, W.H. William, et al., A unified framework for the numerical solution of optimal control problems using pseudospectral methods, Automatica 46 (2010) 1843–1851.

[9] N. Yuya, S. Fumiki, N. Shinichi, Guidance and control of 'tethered retriever' with collaborative tension-thruster control for future on-orbit service missions, in: The 8th International Symposium on Artificial Intelligence: Robotics And Automation in Space—ISAIRAS, Munich, Germany, 2005.

[10] N. Masahiro, Attitude control of a tethered space robot by link motion under microgravity, in: Proceedings of the 2004 IEEE International Conference on Control Applications, Taipei, Taiwan, 2004.

[11] N. Masahiro, D.N. Nenchev, U. Masaru, Tethered robot casting using a spacecraft-mounted manipulator, J. Guid. Control. Dyn. 24 (4) (2001) 827–833.

[12] M. Osamu, M. Saburo, Collaborative control of tethered satellite cluster systems, in: AIAA Guidance, Navigation, and Control Conference and Exhibit, Montreal, Canada, 2001.

[13] K. Godard, D. Kumar, B. Tan, Fault-tolerant stabilization of a tethered satellite system using offset control, J. Spacecr. Rocket. 45 (5) (2008) 1070–1084.

[14] P.E. Gill, W. Murray, M.A. Saunders, SNOPT: an SQP algorithm for large-scale constrained optimization, SIAM J. Optim. 12 (2002) 979–1006.

[15] Y.Z. Luo, G.J. Tang, L.N. Zhou, Simulated annealing for solving near-optimal low-thrust orbit transfer, Eng. Optim. 37 (2) (2005) 201–216.

[16] T.M. Vu, P. John, Fuzzy logic and slip controller of clutch and vibration for hybrid vehicle, Int. J. Control. Autom. Syst. 11 (3) (2013) 526–532.

[17] J. Jin, S. Ko, C.K. Ryoo, Fault tolerant control for satellites with four reaction wheels, Control. Eng. Pract. 16 (2008) 1250–1258.

[18] K.Y. Toumi, S. Reddy, Analysis of linear time invariant systems with time delay, J. Dyn. Syst. Meas. Control. 114 (4) (1992) 544–555.

[19] Y. Jin, P.H. Chang, M. Jin, et al., Stability guaranteed time-delay control of manipulators using nonlinear damping and terminal sliding mode, IEEE Trans. Ind. Electron. 60 (8) (2013) 3304–3317.

[20] A.P. Mohammad, P. Sara, A.N. Mohammad, Stability analysis of time-delayed linear fractional-order systems, Int. J. Control. Autom. Syst. 11 (3) (2013) 519–525.